BIOCHEMISTRY
including biophysical chemistry & molecular biology

Accelerated Publication

pubs.acs.org/biochemistry

Kinetic and Structural Mechanisms of (5′*S*)-8,5′-Cyclo-2′-deoxyguanosine-Induced DNA Replication Stalling

Wenyan Xu,[†] Adam M. Ouellette,[†] Zdzislaw Wawrzak,[§] Storm J. Shriver,[†] Spencer M. Anderson,[§] and Linlin Zhao*[,†,‡]

[†]Department of Chemistry and Biochemistry and [‡]Science of Advanced Materials Program, Central Michigan University, Mount Pleasant, Michigan 48859, United States

[§]Synchrotron Research Center, LS-CAT, Northwestern University, Argonne, Illinois 60439, United States

Supporting Information

ABSTRACT: The (5′*S*)-8,5′-cyclo-2′-deoxyguanosine (*S*-cdG) lesion is produced from reactions of DNA with hydroxyl radicals generated from ionizing radiation or endogenous oxidative metabolisms. An elevated level of *S*-cdG has been detected in Xeroderma pigmentosum, Cockayne syndrome, breast cancer patients, and aged mice. *S*-dG blocks DNA replication and transcription in vitro and in human cells and produces mutant replication and transcription products in vitro and in vivo. Major cellular protection against *S*-dG includes nucleotide excision repair and translesion DNA synthesis. We used kinetic and crystallographic approaches to elucidate the molecular mechanisms of *S*-cdG-induced DNA replication stalling using model B-family *Sulfolobus solfataricus* P2 DNA polymerase B1 (Dpo1) and Y-family *S. solfataricus* P2 DNA polymerase IV (Dpo4). Dpo1 and Dpo4 inefficiently bypassed *S*-cdG with dCTP preferably incorporated and dTTP (for Dpo4) or dATP (for Dpo1) misincorporated. Pre-steady-state kinetics and crystallographic data mechanistically explained the low-efficiency bypass. For Dpo1, *S*-cdG attenuated $K_{d,dNTP,app}$ and k_{pol}. For Dpo4, the *S*-cdG-adducted duplex caused a 6-fold decrease in Dpo4:DNA binding affinity and significantly reduced the concentration of the productive Dpo4:DNA:dCTP complex. Consistent with the inefficient bypass, crystal structures of Dpo4:DNA(*S*-cdG):dCTP (error-free) and Dpo4:DNA(*S*-cdG):dTTP (error-prone) complexes were catalytically incompetent. In the Dpo4:DNA(*S*-cdG):dTTP structure, *S*-cdG induced a loop structure and caused an unusual 5′-template base clustering at the active site, providing the first structural evidence of the previously suggested template loop structure that can be induced by a cyclopurine lesion. Together, our results provided mechanistic insights into *S*-cdG-induced DNA replication stalling.

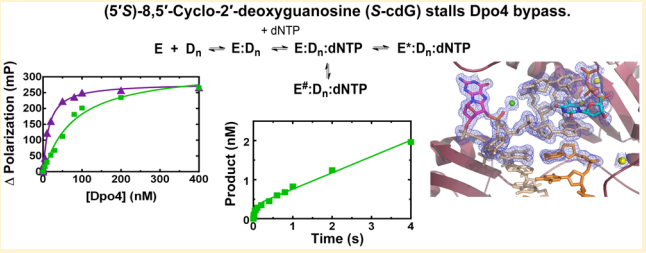

DNA is subject to attack by various sources such as UV and ionizing radiation, environmental pollutants, and endogenous reactive metabolites, producing 50000−100000 DNA modifications per cell each day.[1] Despite the heavy burden of DNA damage, genomic replication is normally an extremely accurate process with an error rate as low as one per 10 billion bases in mammalian cells.[2] The high fidelity is attributed to an intricate defense network including (but not limited to) several high-fidelity DNA polymerases, a complex series of DNA damage response cascades, multifarious DNA repair proteins, and a battery of DNA polymerases specialized for translesion DNA synthesis (TLS).[2] TLS is a major DNA damage tolerance pathway; however, TLS can occasionally introduce errors into a genome. In fact, TLS is responsible for most of the damage-induced point mutations and is thus particularly relevant to the etiology of many human diseases.[3]

Sulfolobus solfataricus P2 (*Sso.*) is an attractive model system for deciphering mechanisms of DNA replication.[4] *Sso.* encodes three B-family DNA polymerases, B1 (Dpo1), B2 (Dpo2), and B3 (Dpo3), and a Y-family DNA polymerase IV (Dpo4).[5,6] Dpo1 is the main replicative DNA polymerase responsible for high-fidelity DNA replication. Dpo1-catalyzed DNA synthesis is blocked at DNA lesions, such as an abasic site and 7,8-dihydro-8-oxo-2′-deoxyguanosine (8-oxodG).[7] Dpo2 and Dpo3 have very low DNA polymerase and 3′ to 5′ exonuclease activities in vitro and can bypass hypoxanthine and 8-oxodG.[5] Dpo4 is an archaeal orthologue of *Escherichia coli* pol IV and human pol κ. Since its crystal structure was first reported in 2001,[8] Dpo4 has been an indispensible tool for understanding TLS in various DNA damage contexts: crystal structures of Dpo4 in complex with a variety of lesion-containing DNA duplexes have been reported, such as ultraviolet-induced photoproduct *cis-syn* cyclobutane pyrimidine dimer,[9] carcinogen benzo[*a*]pyrene diol expoxide-induced DNA adducts,[10] and 8-oxodG (one of the most abundant forms of oxidative DNA damage).[11]

The cyclopurine (CPU) nucleoside adducts are caused by endogenous oxidative stress or ionizing radiation.[12,13] An adenosine adduct was first discovered after adenosine 5′-

Received: December 5, 2014
Revised: January 6, 2015
Published: January 8, 2015

DOI: 10.1021/bi5014936
Biochemistry 2015, 54, 639−651

monophosphate had been exposed to radiation in an oxygen-free aqueous solution.[14] Subsequent studies identified both *R* and *S* diastereoisomers of 8,5′-cyclo-2′-deoxyadenosine (cdA) and 8,5′-cyclo-2′-deoxyguanosine [cdG (*S*-cdG structure shown in Figure 1A)] in DNA after radiation exposure.[15] A major

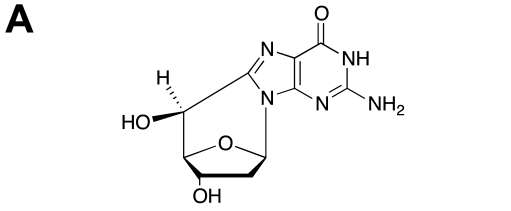

Figure 1. (A) Structure of (5′*S*)-8,5′-cyclo-2′-deoxyguanosine (*S*-cdG). (B) 13/18-mer duplex used for examining the nucleotide incorporation across *S*-cdG or 2′-deoxyguanosine (dG), 14/18-mer duplex used for analyzing the postlesion synthesis, and 13/23-mer duplex used in "running-start" assays.

pathway through which CPU lesions are formed is H-abstraction at C5′ by HO$^{\bullet}$ (generated by radiolysis of water) followed by intramolecular cyclization.[12] Apart from ionizing radiation, the cdA and cdG lesions are DNA damage products from endogenous reactive oxygen species. The cdA adduct was first identified as one of the dinucleotides termed "type II I-compounds" in aged rodents using a ^{32}P postlabeling technique.[16] Subsequently, using isotope dilution mass spectrometry, an increasing level of all four diastereoisomers was observed in aged rodents in a tissue specific manner,[17,18] and in mice under inflammatory conditions.[19,20] More recently, CPU lesions were also found to accumulate in ultraviolet radiation-independent mouse melanoma,[21] and Xeroderma pigmentosum, Cockayne syndrome, breast cancer, and familial Mediterranean fever patients,[12,22−24] underscoring the importance of CPU lesions in disease processes.

Unlike many other oxidative DNA damage lesions, the CPU lesions are resistant to base excision repair (BER).[25−28] Although CPU lesions are substrates for nucleotide excision repair (NER), the rate of incision of *S*-cdG by *E. coli* UvrABC NER proteins is only $^{1}/_{10}$ of the rate of a typical NER substrate, the C8-dG adduct of *N*-acetyl-2-aminofluorene.[29] The 5′*S* isomers are more resilient to NER than the 5′*R* isomers for both cdA and cdG,[25,30] also evidenced by a higher level of 5′*S* isomers than 5′*R* isomers detected in mice.[18] Unrepaired and accumulated CPU lesions are strong blocks to DNA replication and transcription in vitro and in human cells[25,31] and can induce the formation of mutant replication and transcription products in vivo.[29,32] A common mutation pattern found for *S*-cdG includes G → A transition and G → T transversion mutations with varying mutation frequencies in *E. coli* and human cells.[29,32] In vitro studies found cdG is bypassed by *E. coli* pol IV, human polymerases κ and ζ, and Dpo4 in an inefficient and highly error-prone fashion but can be bypassed by human pol η and pol ι in a largely error-free fashion.[32,33] Structural attributes of CPU lesions potentially contribute to their mutagenic and DNA repair resistance properties. An unusual O4′-*exo* sugar puckering for the CPU lesions and substantial changes in backbone torsion angles have been observed in nuclear magnetic resonance (NMR) structures of duplex DNA containing 5′*S* isomers of cdA and cdG.[34−36] Molecular modeling and dynamic simulations showed a higher degree of perturbations caused by 5′*R* lesions could contribute to their greater NER incision susceptibility.[30] These studies provided important information about structural perturbations imposed by these lesions in a DNA duplex. However, the molecular basis for how CPU lesions induce mutagenic DNA polymerase bypass or DNA polymerase stalling remains elusive.

Herein we used *S*-cdG as a representative CPU lesion and Dpo1 and Dpo4 as model replicative and TLS pols to elucidate the mechanisms of DNA replication stalling induced by *S*-cdG. Steady-state and pre-steady-state kinetic assays were used to pinpoint the microscopic kinetic steps affected by the presence of *S*-cdG during DNA replication. Two high-resolution X-ray crystal structures of Dpo4 revealed, from a structural perspective, how *S*-cdG hindered DNA replication. Our study provides, for the first time, kinetic and structural insights into the mutagenic bypass of *S*-cdG.

EXPERIMENTAL PROCEDURES

Materials. All commercial chemicals were of the highest quality available and were used without further purification. Unlabeled dNTPs and T4 polynucleotide kinase were from New England Biolabs (Ipswich, MA). [γ-^{32}P]ATP (specific activity of 3×10^3 Ci mmol^{-1}) was from PerkinElmer Life Sciences (Boston, MA) or MP Biomedicals (Santa Ana, CA). Oligonucleotides containing *S*-cdG were synthesized and purified by high-performance liquid chromatography (HPLC) by TriLink Biotechnologies (San Diego, CA). The purity of the lesion-containing oligonucleotides was shown by polyacrylamide gel electrophoresis to be >99% by the manufacturer. The molecular weight was confirmed by MALDI mass spectrometry: 18-mer-*S*-cdG, found *m*/*z* 5351.9, calcd *m*/*z* 5353.6; 23-mer-*S*-cdG, found *m*/*z* 7063.3, calcd *m*/*z* 7063.4. Other oligonucleotides were from Integrated DNA Technologies (Coralville, IA) and purified by HPLC. Dpo4 and Dpo1 [exo^{-}, triple mutant (D231A/E233A/D318A)] expression vectors were kindly provided by F. P. Guengerich (Vanderbilt University School of Medicine, Nashville, TN). Both proteins were expressed and purified as described previously.[37] The 3′ → 5′ exonuclease-deficient mutant of Dpo1 was used to avoid complication in interpreting the kinetic data of nucleotide incorporation.

Primer Extension and Steady-State Kinetic Assays. A DNA duplex (sequences shown in Figure 1B) with a 5′-[γ-^{32}P]ATP end label on the primer was annealed to a template with dG or *S*-cdG. Primer extension assays were performed in 40 mM Tris-HCl buffer (pH 7.4) containing 100 nM primer−template complex, 50 μM dNTPs, 100 or 50 nM polymerase,

DOI: 10.1021/bi5014936
Biochemistry 2015, 54, 639−651

5% (v/v) glycerol, 3 mM DTT, 40 mM NaCl, 5 mM $MgCl_2$, and 50 μg mL^{-1} bovine serum albumin (BSA) at 37 °C. Steady-state kinetic experiments were conducted under the same conditions except using 0.5−10 nM pol at varying dNTP concentrations and incubation times (3−10 min). Reactions were quenched by adding 1.5 μL of reaction mixture to 9 μL of 20 mM EDTA (pH 9.0) in 95% (v/v) formamide. After denaturation at 90 °C, reaction products were rapidly cooled on ice and separated using 16% (w/v) acrylamide gel electrophoresis containing 7 M urea. Results were visualized using a phosphorimaging system (GE Healthcare, Typhoon FLA7000) and analyzed with ImageQuant. Data were fit to the Michaelis−Menten equation to obtain k_{cat} and K_m using Prism (GraphPad, San Diego, CA).

DNA Polymerase−DNA Binding Affinity. A fluorescein amidite (FAM)-labeled 13/18-mer duplex (10 nM) was incubated with varying concentrations of Dpo1 or Dpo4 (0.5−400 nM) for 30 min at 37 °C, followed by fluorescence polarization measurements performed on an Infinite F200 Pro microplate reader (TECAN US Inc., Durham, NC) using filter sets with a λ_{ex} of 485 nm and a λ_{em} of 525 nm. All titrations were performed in 50 mM HEPES buffer (pH 7.4) containing 10 mM potassium acetate, 5 mM $MgCl_2$, 2 mM β-mercaptoethanol, and 100 μg mL^{-1} BSA. Data were acquired at 37 °C and then fit to a quadratic equation to estimate $K_{d,DNA}$, using a quadratic equation

$$y = F + 0.5D(P - F)\{K + x + D - [(K + x + D)^2 - 4Dx]^{1/2}\} \quad (1)$$

where x is the concentration of DNA polymerase, y is the change in fluorescence polarization (ΔmP), K is the equilibrium dissociation constant ($K_{d,DNA}$) for DNA polymerase−DNA binding, P is the maximal polarization, and F is the initial polarization.[38]

Pre-Steady-State Kinetics. Pre-steady-state kinetic assays were performed on a KinTek RQF-3 model chemical quench-flow apparatus (KinTek Corp., Austin, TX). Burst kinetic experiments were conducted under enzyme-limiting conditions by rapid mixing of 50 nM primer−template duplex and pols with 1 mM dCTP. All concentrations are final concentrations after mixing. Reactions were quenched by mixing samples with 0.3 M EDTA. Assays contained 12.5−50 nM Dpo1 (or Dpo4), 5% (v/v) glycerol, 3 mM DTT, 40 mM NaCl, 5 mM $MgCl_2$, and 50 μg mL^{-1} BSA in 40 mM Tris-HCl buffer (pH 7.4). Data were fit to a burst equation

$$y = A(1 - e^{-k_{obs}t}) + k_{ss}t \quad (2)$$

where A is the product amplitude following the first binding event, k_{obs} is the rate of polymerization, k_{ss} is the steady-state rate of nucleotide incorporation, and t is the reaction time. The maximal single-nucleotide incorporation rate constant (k_{pol}) and the apparent nucleotide dissociation constant ($K_{d,dCTP,app}$) from a kinetically active ternary complex were measured in the presence of excess DNA polymerase with a series of dCTP concentrations (0.5−2400 μM). Under single-turnover conditions, time-dependent product formation at each dCTP concentration was fit to a single-exponential equation

$$y = A(1 - e^{-k_{obs}t}) \quad (3)$$

where A is the product amplitude following the first binding event, k_{obs} is the rate of polymerization, and t is the reaction time. The obtained k_{obs} values were plotted as a function of dCTP concentration and fit to a hyperbolic equation

$$y = k_{pol}[dCTP]/(K_{d,dCTP,app} + [dCTP]) \quad (4)$$

The product amplitude (A) for the Dpo4-catalyzed dCTP insertion opposite *S*-cdG was dependent on the dCTP concentration and was fit to eq 4 to obtain $K_{d,dCTP,app}$.[39]

Crystallization of Dpo4:*S*-cdG:dNTP Complexes. The 13/18-mer duplex used for cocrystallization with Dpo4 is shown in Figure 1B except that the 3′-terminal C was a 2′,3′-dideoxycytidine to prevent polymerization. Crystals were obtained under similar conditions as described previously.[40] Specifically, the Dpo4:*S*-cdG:dCTP complex was crystallized in a solution of 220 μM Dpo4, 264 μM 13/18-mer duplex, 5 mM $MgCl_2$, 1 mM dCTP, 20 mM Tris-HCl (pH 7.4), 60 mM NaCl, 2% (v/v) glycerol, and 5 mM β-mercaptoethanol mixed in a 1:1 (v/v) ratio with a reservoir solution containing 0.1 M Tris-HCl (pH 7.4), 15% (w/v) polyethylene glycol 3350, 0.1 M $Ca(CH_3COO)_2$, and 2% (v/v) glycerol. The Dpo4:*S*-cdG:dTTP crystals were obtained with 180 μM Dpo4, 216 μM 13/18-mer duplex, and 1 mM dTTP, with concentrations of other components that were the same as in the crystallization of the Dpo4:*S*-cdG:dCTP complex. Crystals were grown using the hanging-drop vapor diffusion method at 19 °C. Crystals were harvested and soaked in a mother liquor solution containing 25% (w/v) polyethylene glycol 3350 and 15% (v/v) ethylene glycol prior to being flash-frozen in liquid nitrogen.

Structure Determination and Refinement. X-ray diffraction data were collected on the 21-ID-F beamline at the Advanced Photon Source (Argonne National Laboratory, Argonne, IL). All data sets were recorded from cryoprotected crystals using a single wavelength at 100 K. Data were indexed and scaled with HKL2000.[41] X-ray diffraction data collection and processing statistics are listed in Table 5. For the Dpo4:*S*-cdG:dTTP complex, molecular replacement with MOLREP[42] was performed on the basis of a previous Dpo4 model [Protein Data Bank (PDB) entry 2IMW].[43] For the Dpo4:*S*-cdG:dCTP complex, crystals were twinned and processed in $P2_1$ with the twinning law. Phases were calculated using ARP/wARP as part of the CCP4 program suite.[44,45] Both crystal complexes were refined in Phenix (1.9.1690).[46] Repeated cycles of manual rebuilding were performed in COOT.[47] Structural images were generated in PyMOL.[48]

RESULTS

***S*-cdG Was a Strong Block for Dpo1- and Dpo4-Catalyzed DNA Replication.** Primer extension assays were performed first to examine the bypass capabilities of Dpo1 and Dpo4. A "running-start" assay with 13/23-mer (sequence shown in Figure 1B) showed that DNA synthesis was markedly stalled at the position opposite *S*-cdG for Dpo1 (Figure 2A, lanes 5 and 6) and moderately stalled for Dpo4 (Figure 2A, lanes 11 and 12). Dpo1, a replicative DNA polymerase, was incapable of extending the primer to a full length product, whereas Dpo4 moderately passed *S*-cdG to produce a low level of full length product(s). A "standing-start" assay with 13/18-mer duplexes containing dG or *S*-cdG (sequence shown in Figure 1B) demonstrated a similar stalling effect imposed by *S*-cdG for Dpo1 (Figure 2B, lanes 14 and 20) and Dpo4 (Figure 2A, lanes 20 and 21). On the other hand, efficient primer extensions were observed with undamaged templates (Figure 2, lanes 2, 3, 17, and 18 for Dpo1 and lanes 8, 9, 23, and 24 for

DOI: 10.1021/bi5014936
Biochemistry 2015, 54, 639−651

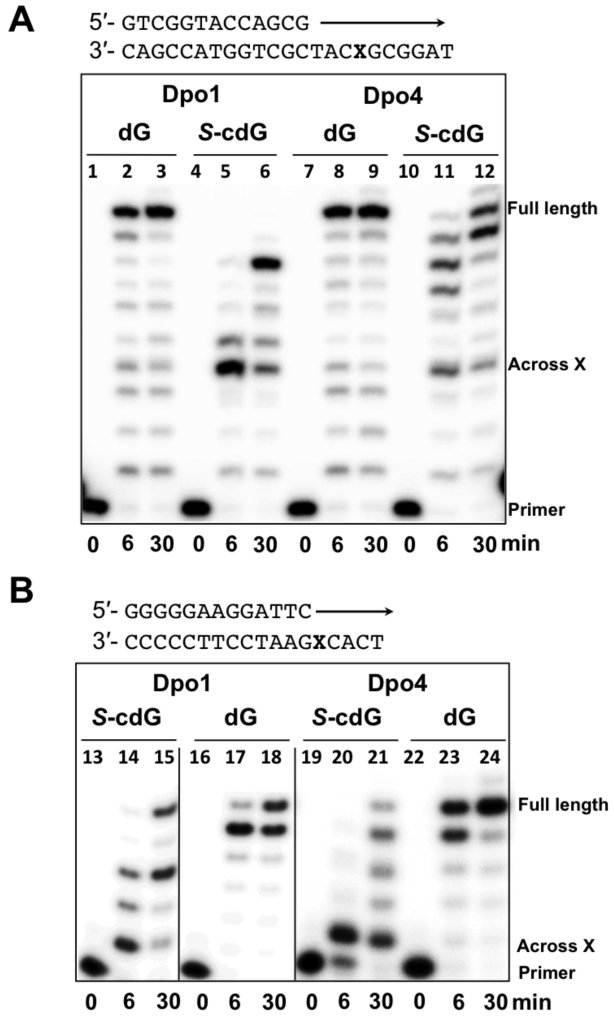

Figure 2. Primer extension experiments examining the bypass of template (5′*S*)-8,5′-cyclo-2′-deoxyguanosine (*S*-cdG) or 2′-deoxyguanosine (dG) catalyzed by Dpo1 or Dpo4. (A) "Running-start" primer extension assays with 50 nM Dpo1 or Dpo4. (B) "Standing-start" primer extension assays with 50 nM Dpo1 or Dpo4. Assays were performed at 37 °C and contained 100 nM primer–template complex, 50 μM dNTPs, 50 nM Dpo1 (or Dpo4), 5% (v/v) glycerol, 3 mM DTT, 40 mM NaCl, 5 mM $MgCl_2$, and 50 μg mL^{-1} BSA in 40 mM Tris-HCl (pH 7.4).

Dpo4). Moderate bypass was achieved with a longer reaction time (30 min) or a higher enzyme concentration (100 nM) (Figure S2 of the Supporting Information). Overall, *S*-cdG was a strong block for Dpo1- and Dpo4-catalyzed DNA replication, consistent with the stalling effects observed previously with other B-family and Y-family DNA polymerases.[25,32]

S-cdG Bypass by Dpo1 or Dpo4 Was Error-Prone and Inefficient. Steady-state kinetic assays were used to analyze the catalytic efficiency and error frequency of *S*-cdG bypass. Both Dpo1 and Dpo4 preferred to incorporate the correct C across the template *S*-cdG, although the process was equally inefficient for both pols (Table 1, k_{cat}/K_m within a factor of 2). Compared to that of the undamaged G:dCTP pair, 140- and 65-fold decreases in the catalytic specificity constant (k_{cat}/K_m) were observed for Dpo1 and Dpo4, respectively. *S*-cdG bypass by Dpo1 or Dpo4 was error-prone. Dpo1 misincorporated dATP opposite the template *S*-cdG with a frequency (0.11) higher than that with dTTP (0.02) or dGTP (0.002); Dpo4 showed an error frequency of 0.36 for the *S*-cdG:dTTP mispair, 0.09 for the *S*-cdG:dATP mispair, and 0.026 for the *S*-cdG:dGTP mispair. A similar mutation pattern was observed for Dpo4 with a different sequence context [G on the 5′ side of *S*-cdG (Table S1 of the Supporting Information)]. Together, our results demonstrated that bypass of *S*-cdG was inefficient for Dpo1 and Dpo4, and the lesion induced mutagenic mispairs.

S-cdG Weakened Dpo4–DNA Binding but Not Dpo1–DNA Binding. Previous solution NMR structures have shown that CPU lesions give rise to significant distortions in the DNA duplex.[34−36] These results prompted us to investigate the potential effect on DNA–pol binding that might be caused by these structural distortions. We conducted fluorescence polarization experiments using a fluorescein-labeled primer annealed to a template containing dG or *S*-cdG to obtain the equilibrium dissociation constant ($K_{d,DNA}$) for Dpo1 and Dpo4 (Figure 3). $K_{d,DNA}$ values with an unmodified template were 6.5 ± 1.7 and 13 ± 2 nM for Dpo1 and Dpo4, respectively, in agreement with literature values obtained by gel mobility shift assays.[49] Interestingly, the *S*-cdG-harboring duplex resulted in a similar $K_{d,DNA}$ (8.6 ± 1.8 nM) with Dpo1 compared to a value of 6.5 ± 1.7 nM with an unmodified duplex, suggesting that the presence of *S*-cdG in the template did not perturb Dpo1–DNA binding. By contrast, *S*-cdG resulted in an approximately 6-fold higher $K_{d,DNA}$ for Dpo4, suggesting that structural disruption imposed by *S*-cdG weakened Dpo4–DNA binding, which contributes in part to the 65-fold decrease seen for Dpo4 in the level of dCTP catalysis (*vide supra*, steady-state kinetics). Thus, our data demonstrated that structural disruptions potentially imposed by the template *S*-cdG weakened Dpo4–DNA binding.

S-cdG Compromised the Formation of a Productive Dpo4:DNA:dCTP Complex. Steady-state kinetics provides the overall efficiency on a single catalytic cycle but does not offer details about individual catalytic steps. Pre-steady-state kinetics is powerful in dissecting the catalytic mechanisms of an enzyme.[38] We used pre-steady-state burst kinetics (or active site titration) to examine the transient concentration of the productive pol:DNA:dNTP complex during catalysis (Figure 4 and Table 2). This concentration is important for defining the active portion of the enzyme in a certain protein preparation, and it is also meaningful in explaining the partition between the productive and nonproductive complexes during TLS.[38,50] Dpo4-catalyzed DNA synthesis across template G gave a burst amplitude that is stoichiometric with enzyme concentration (98%), whereas Dpo1 gave an amplitude that is approximately half of the total enzyme (56%), perhaps because of the mutant Dpo1 used. These results suggest that all (for Dpo4) or nearly all (for Dpo1) enzymes formed productive complexes with an unmodified DNA duplex. For the error-free bypass by Dpo1, the percentage of productive complex with an *S*-cdG-bearing duplex decreased to approximately half of that for an unmodified DNA duplex. Remarkably, *S*-cdG reduced the concentration of productive complex to only ~1% of the total concentrations of the enzyme, suggesting that *S*-cdG had a major impact on Dpo4 catalysis, rendering a majority of the Dpo4:DNA:dNTP complex catalytically inactive. Together, results from pre-steady-state burst kinetic assays supported the low k_{cat}/K_m seen in steady-state kinetic assays.

S-cdG Decreased k_{pol} and Increased $K_{d,dCTP,app}$ for Dpo1 but Not for Dpo4. Pre-steady-state kinetics under single-turnover conditions allowed us to determine key kinetic parameters, such as the maximal polymerization rate (k_{pol}), the

DOI: 10.1021/bi5014936
Biochemistry 2015, 54, 639–651

Table 1. Steady-State Kinetic Parameters for Single-Nucleotide Incorporations opposite (5′*S*)-8,5′-Cyclo-2′-deoxyguanosine (*S*-cdG) or 2′-Deoxyguanosine (dG) Catalyzed by Dpo1 or Dpo4[a]

polymerase	template:dNTP pair	k_{cat} (min^{-1})	$K_{m,dNTP}$ (μM)	$k_{cat}/K_{m,dNTP}$ (min^{-1} μM^{-1})	f^b	change in specificity relative to dG:C[c]
Dpo1	*S*-cdG:C	0.25 ± 0.03	6.8 ± 1.2	0.036		140-fold lower
	S-cdG:T	0.013 ± 0.001	18 ± 5	0.00072	0.020	
	S-cdG:A	0.46 ± 0.04	120 ± 20	0.0038	0.11	
	S-cdG:G	0.093 ± 0.008	1020 ± 150	0.000091	0.0025	
	dG:C	3.7 ± 0.2	0.71 ± 0.06	5.2		
	dG:T	2.7 ± 0.7	780 ± 280	0.0035	0.00067	
	dG:A	0.17 ± 0.03	120 ± 40	0.0014	0.00027	
	dG:G	0.023 ± 0.001	16 ± 4	0.0014	0.00027	
Dpo4	*S*-cdG:C	1.6 ± 0.1	80 ± 9	0.020		65-fold lower
	S-cdG:T	2.8 ± 0.3	380 ± 80	0.0074	0.37	
	S-cdG:A	1.1 ± 0.1	620 ± 50	0.0018	0.090	
	S-cdG:G	0.46 ± 0.02	900 ± 70	0.00051	0.026	
	dG:C	2.4 ± 0.1	1.9 ± 0.2	1.3		
	dG:T	1.6 ± 0.1	780 ± 70	0.0021	0.0016	
	dG:A	0.61 ± 0.04	920 ± 110	0.00066	0.00051	
	dG:G	0.29 ± 0.01	320 ± 40	0.00091	0.00070	

[a]The assays were performed at 37 °C with 100 nM 13/18-mer duplex, varying dNTP concentrations, 0.5−10 nM DNA polymerase, 5% (v/v) glycerol, 3 mM DTT, 40 mM NaCl, 5 mM $MgCl_2$, and 50 μg mL^{-1} bovine serum albumin (BSA) in 40 mM Tris-HCl buffer. [b]Misinsertion frequency $f = (k_{cat}/K_{m,dNTP})_{incorrect}/(k_{cat}/K_{m,dCTP})_{correct}$. [c]Change of specificity, calculated from $(k_{cat}/K_m)_{S\text{-}cdG:C}/(k_{cat}/K_m)_{dG:C}$.

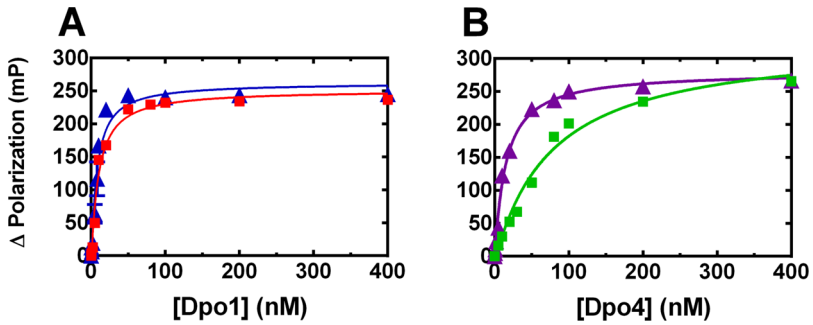

Figure 3. Effect of the adduct-containing template on the equilibrium dissociation constant ($K_{d,DNA}$) of (A) Dpo1 and (B) Dpo4. Fluorescence anisotropy assays contained FAM-labeled 13/18-mer duplex (10 nM) and varying concentrations of Dpo1 or Dpo4 (0.5−400 nM), followed by fluorescence polarization measurements. The different templates are 13/18-mer(*S*-cdG) (■) and 13/18-mer(dG) (▲). All titrations were performed in 50 mM HEPES buffer (pH 7.4) containing 10 mM potassium acetate, 5 mM $MgCl_2$, 2 mM β-mercaptoethanol, and 0.1 μg mL^{-1} BSA. Data were fit to a quadratic equation (eq 1 in Experimental Procedures) to obtain $K_{d,DNA}$ values 8.6 ± 1.8 nM [Dpo1 with 13/18-mer(*S*-cdG)], 6.5 ± 1.7 nM [Dpo1 with 13/18-mer(dG)], 76 ± 16 nM [Dpo4 with 13/18-mer(*S*-cdG)], and 13 ± 2 nM [Dpo4 with 13/18-mer(dG)].

apparent nucleotide dissociation constant from a kinetically active ternary complex ($K_{d,dCTP,app}$), and the catalytic efficiency ($k_{pol}/K_{d,dCTP,app}$). For Dpo1-catalyzed error-free bypass (Table 3 and Figure S2A−D of the Supporting Information), the catalytic efficiency was 100-fold lower than that of an unmodified dG:dCTP pair, which explained the 140-fold attenuation seen in k_{cat}/K_m in the steady-state kinetic results. This decrease, deriving from a 4-fold decrease in k_{pol} and a 27-fold increase in $K_{d,dCTP,app}$ for the *S*-cdG:dCTP pair compared to those of the dG:dCTP pair, suggests that *S*-cdG attenuated nucleotide incorporation due to weakened nucleotide binding and a lowered k_{pol} [function of the rate of the forward conformational change and the chemistry step (see Discussion)].[38]

The Dpo4-catalyzed dCTP incorporation opposite *S*-cdG (Table 3 and Figure S2E,F of the Supporting Information) was somewhat unusual in that its k_{pol} was independent of the dCTP concentration (Figure S2F of the Supporting Information, inset). Instead, the product amplitude was dependent on the dCTP concentration (Figure S2F of the Supporting Information), which suggests that the polymerization is readily reversible, so that the increase in dCTP concentration drives an increasing amount of product formed at the enzyme active site.[39] On the basis of the product amplitude dependence, $K_{d,dCTP,app}$ was estimated to be 139 ± 36 μM for the *S*-cdG:dCTP pair, which was similar to the value of 150 ± 40 μM for the dG:C pair, suggesting the *S*-cdG-containing pair did not alter the apparent nucleotide dissociation constant. We estimated k_{pol} to be 43 ± 20 s^{-1} based upon the highest k_{obs} obtained. Thus, the catalytic efficiency $k_{pol}/K_{d,dCTP,app}$ was 0.31 s^{-1} μM^{-1} for the *S*-cdG:dCTP pair, ~15-fold higher than that for the normal dG:dCTP pair. The higher catalytic efficiency observed for the adducted template does not contradict the decrease in specificity constant for dCTP in the aforementioned steady-state kinetic results. This is because $k_{pol}/K_{d,dCTP,app}$ is a more precise measure of catalytic events during the nucleotide binding, pol conformation change, and nucleotidyl transfer steps (Scheme 1), whereas k_{cat}/K_m measured in steady-state kinetics is a function of kinetic constants of all steps in a single catalytic cycle, including a conformational relaxation step after the nucleotidyl transfer, which is the rate-limiting step for Dpo4.[50] Therefore, through

DOI: 10.1021/bi5014936
Biochemistry 2015, 54, 639−651

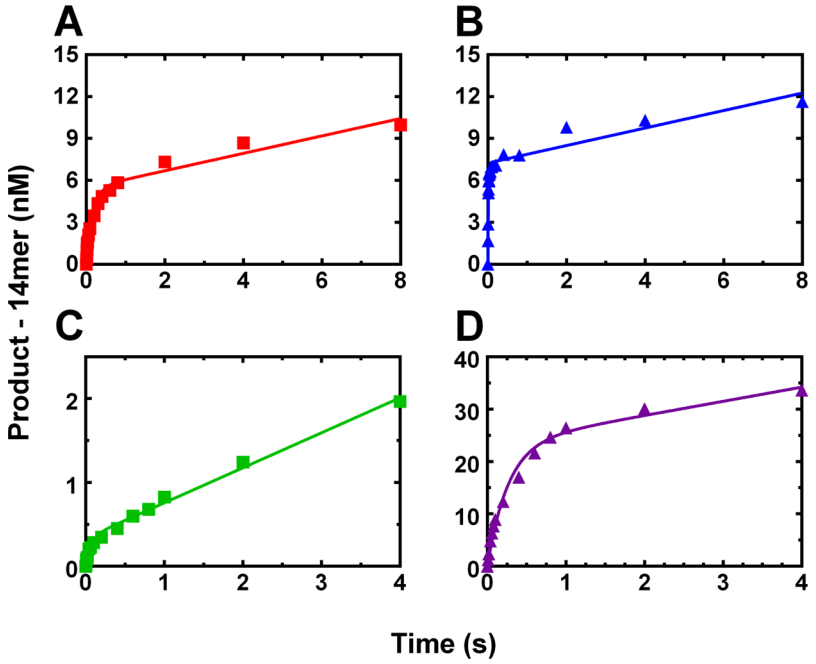

Figure 4. Effect of the adduct-containing template on the transient concentration of the productive pol:DNA:dNTP complex. Pre-steady-state burst kinetic assays were performed under enzyme-limiting conditions. (A) Dpo1 (16 nM) with 13/18-mer(*S*-cdG), (B) Dpo1 (12.5 nM) with 13/18-mer(dG), (C) Dpo4 (25 nM) with 13/18-mer(*S*-cdG), and (D) Dpo4 (25 nM) with 13/18-mer(dG). Assays were initiated by rapid mixing of the preformed pol:DNA complex (50 nM duplex and varying concentrations of pol) with 1 mM dCTP and terminated by mixing with 0.3 M EDTA. All concentrations were final concentrations after mixing. Assays contained 5% (v/v) glycerol, 3 mM DTT, 40 mM NaCl, 5 mM $MgCl_2$, and 50 μg mL^{-1} BSA in 40 mM Tris-HCl buffer (pH 7.4). Data were fit to a double-exponential equation (eq 2 in Experimental Procedures), and results are summarized in Table 2.

Table 2. Pre-Steady-State Burst Kinetic Parameters for Single-Base Incorporation opposite (5′*S*)-8,5′-Cyclo-2′-deoxyguanosine (*S*-cdG) or 2′-Deoxyguanosine (dG) Catalyzed by Dpo1 or Dpo4[a]

polymerase	template:dNTP pair	k_{obs} (s^{-1})	k_{ss} (s^{-1})	A[b] (nM)	[productive]/[total][c] (%)
Dpo1	*S*-cdG:C	6.0 ± 1.0	0.62 ± 0.08	5.4 ± 0.3	33
	dG:C	69.9 ± 5.8	0.94 ± 0.10	7.0 ± 0.1	56
Dpo4	*S*-cdG:C	15.0 ± 3.7	0.42 ± 0.01	0.34 ± 0.03	1.4
	dG:C	3.8 ± 0.5	2.7 ± 0.5	23.4 ± 1.4	94

[a]See the legend of Figure 4 for experimental conditions. Data were fit to eq 2 in Experimental Procedures. [b]A is the product amplitude. [c]Values were obtained by dividing the product amplitude by the total enzyme concentration in each assay.

Table 3. Effect of the *S*-cdG-Containing Template on the Maximal Polymerization Rate (k_{pol}) and the Apparent Nucleotide Dissociation Constant ($K_{d,dCTP,app}$) for the Incorporation of the Correct Base (dCTP)[a]

polymerase	template:dNTP pair	k_{pol} (s^{-1})	$K_{d,dCTP,app}$ (μM)	$k_{pol}/K_{d,dCTP,app}$ (s^{-1} μM^{-1})
Dpo1	*S*-cdG:C	2.6 ± 0.4	620 ± 200	0.0042
	dG:C	9.9 ± 0.9	23 ± 7	0.43
Dpo4	*S*-cdG:C	43 ± 20	139 ± 36	0.31
	dG:C	3.0 ± 0.2	150 ± 40	0.020

[a]Pre-steady-state kinetic assays were performed under single-turnover conditions with limiting DNA duplexes. Data were obtained by rapid mixing of 50−100 nM primer−template duplex and 250 nM to 20 μM DNA polymerase with varying concentrations of dCTP (0.5−2400 μM). See Figure S3 of the Supporting Information for concentrations of pols. Assays contained 5 mM $MgCl_2$, 5% (v/v) glycerol, 3 mM DTT, 40 mM NaCl, and 50 μg mL^{-1} bovine serum albumin (BSA) in 40 mM Tris-HCl buffer (pH 7.4). Data were fit to eq 3 (Experimental Procedures) to obtain k_{obs}, which was then fit to eq 4 as a function of dCTP concentration. For Dpo4-catalyzed dCTP insertion opposite *S*-cdG, the product amplitude and dCTP concentration were fit to eq 4.

pre-steady-state kinetic analysis, we gained a mechanistic view of the effect of *S*-cdG on Dpo1 and Dpo4 catalysis. The 140-fold decrease in dCTP catalytic efficiency for Dpo1 when encountering *S*-cdG can be explained by the decrease in the maximal polymerization rate (k_{pol}) and the increase in the apparent nucleotide dissociation constant ($K_{d,dCTP,app}$). For Dpo4-catalyzed error-free *S*-cdG bypass, the 65-fold attenuation of the specificity constant of dCTP is caused in part by the 100-fold decrease in the concentration of the productive Dpo4:DNA:dCTP complex.

Postlesion DNA Synthesis beyond the *S*-cdG:dCMP Pair Was Very Inefficient for Dpo1 and Dpo4. To assess the extension efficiency beyond the damaged site, we conducted primer extensions with a 14/18-mer with an *S*-cdG:dCMP pair (see Figure 1B for the duplex sequence and Figure S3 of the Supporting Information for the extension assays). The catalytic specificity constant for the correct dGTP was obtained for templates containing *S*-cdG or dG, as summarized in Table 4. Consistent with the inefficient primer extension pattern in Figure 2, the postlesion synthesis was inefficient for Dpo1 and Dpo4 (Figure S3 of the Supporting

DOI: 10.1021/bi5014936
Biochemistry 2015, 54, 639−651

Scheme 1. Minimal Kinetic Model of DNA Polymerase Catalysis

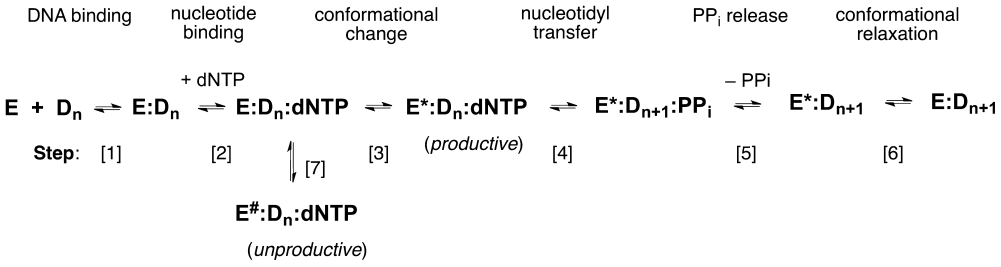

Table 4. Steady-State Kinetic Parameters for Dpo1- and Dpo4-Catalyzed Postlesion Extension[b]

Polymerase	Template	k_{cat} (min^{-1})	$K_{m,dGTP}$ (μM)	$k_{cat}/K_{m,dGTP}$ (min^{-1} $μM^{-1}$)	$k_{cat}/K_{m,dGTP}$ decrease relative to an unmodified template [a]
Dpo1	5′---------C 3′-(*S*-cdG)C	0.21 ± 0.02	710 ± 120	0.00030	200-fold
	5′----C 3′-(dG)C	0.56 ± 0.02	11 ± 1	0.051	
Dpo4	5′---------C 3′-(*S*-cdG)C	0.09 ± 0.01	1500 ± 200	0.00006	3000-fold
	5′----C 3′-(dG)C	3.6 ± 0.3	18 ± 2.7	0.2	

[a]Change in specificity, calculated from $(k_{cat}/K_m)_{dGTP,damaged}/(k_{cat}/K_m)_{dGTP,unmodified}$. [b]A 14/18-mer duplex (sequence shown in Figure 1B) was used for analyzing the incorporations of dGTP opposite the template C at the 5′ position of (5′*S*)-8,5′-cyclo-2′-deoxyguanosine (*S*-cdG) or 2′-deoxyguanosine (dG).

Information). A decline in the dGTP specificity constant was seen for Dpo1 and Dpo4 in the postlesion incorporation event, i.e., 200-fold decrease for Dpo1 and 3000-fold decrease for Dpo4. Compared to that of Dpo4, Dpo1 showed a 5-fold higher catalytic specificity constant of dGTP, suggesting that Dpo1 may be a major player in post-*S*-cdG DNA synthesis in vivo.

Dpo4 Crystal Structures Supported the Existence of Catalytically Inactive Complexes. To understand the structural mechanisms of *S*-cdG-induced DNA replication stalling and inefficient bypass, we determined two ternary structures of Dpo4 at high resolutions capturing the error-free (*S*-cdG:dCTP) and error-prone (*S*-cdG:dTTP) bypass. The Dpo4:*S*-cdG:dCTP and Dpo4:*S*-cdG:dTTP complexes are designated as Dpo4-1 (refined to 2.06 Å) and Dpo4-2 (refined to 1.58 Å), respectively. Crystallographic data collection and refinement statistics are listed in Table 5. The overall architecture of Dpo4-1 (Figure 5A) was similar to that of the previously reported "type I" Dpo4 ternary structure [PDB entry 2AGQ, Cα root-mean-square deviation (rmsd) of 1.017 Å].[8] The protein structure (without DNA) closely resembled the Dpo4 structure featuring the error-free bypass of 8-oxodG[51] (PDB entry 2C2R, Cα rmsd of 0.595 Å, superimposed structures shown Figure 5B). A close-up view of the active site revealed that *S*-cdG was shifted toward the major groove. Incomplete electron density was observed for *S*-cdG, i.e., partial electron density for the sugar pucker and a part of the pyrimidine ring and complete electron density for the phosphate group (omit map shown at the 1σ level in Figure 6A). However, the existing map confirmed the identity of *S*-cdG because of the clear electron density seen for the covalent linkage between the C5′ atom and the C8 atom (unique for *S*-cdG). The observed electron density map suggests *S*-cdG interacts with surrounding amino acid residues and ions. Indeed, the exocyclic N2 atom of *S*-cdG interacted with the carbonyl O atom of Gly58 and a water molecule via hydrogen binding (Figure 6C). The N3 atom of the pyrimidine ring formed a hydrogen bond with a different water molecule.

The incoming dCTP was paired with a template G at position −1 via Watson−Crick base pairing (Figure 6B), and the C^{dd} at the primer terminus bulged to the minor-groove side. The conformation with a bulged out primer C^{dd} positioned in the minor groove was also seen in several reported Dpo4 structures.[51,52] The distance between the C3′ atom of primer terminal C^{dd} and the α-phosphate atom of dCTP was 9.2 Å, rendering the complex catalytically incompetent. The inactive state is consistent with the low catalytic efficiency of insertion of dCTP opposite *S*-cdG catalyzed by Dpo4. As noted earlier in the pre-steady-state kinetic results, the nucleotidyl transfer step for the Dpo4-catalyzed dCTP insertion could be readily reversible. It is conceivable that the structure observed here may represent the stage after a conformational change from a catalytically active state.

In contrast to Dpo4-1, Dpo4-2 (Dpo4:*S*-cdG:dTTP) showed large deviations (Cα rmsd of 3.183 Å) from a "type I" Dpo4 structure (Figure 5C and the structure colored red in Figure 5D). A looped template was observed possibly induced by an unusual sugar puckering of 8,5′-cyclization of *S*-cdG.[53] As a result, an unexpected clustering of three template bases (A, C, and T at positions +2, +3, and +4, respectively) was seen at the active site, causing a wider opening between the little finger and finger domains [structure colored red compared to the structure colored green (PDB entry 2C2R) in Figure 5D]. The pyrimidine ring and sugar residues of the incoming dTTP were shifted to the major-groove side, though the phosphate groups were still stabilized by magnesium chelation (Figure 6D). The phosphate groups of dTTP adopted a "goat-tail"-like conformation somewhat similar to that observed in a Dpo4 complex containing a mismatch.[54] The *S*-cdG lesion is stabilized via Ca^{2+} chelation and hydrogen bonds with several water molecules (Figure 6F). The metal ion was refined as Ca^{2+} instead of Mg^{2+} because of the presence of 0.05 M $Ca(CH_3COOH)_2$ under crystallization conditions and a total seven ligands observed with an average distance of 2.4 Å to the metal ion (Figure 6E).[55] The pyrimidine ring of template C at position +3 interacted via π−π stacking with Tyr12, which would otherwise interact with the sugar pucker of the incoming nucleotide. The template C at position +3 displaced the pyrimidine ring and the sugar pucker of dTTP from the typical position of an incoming nucleotide in a "type I" Dpo4 structure (Figure 6D,F). Notably, the pyrimidine ring and sugar pucker were flipped 180° compared to those of a normal conformation of the incoming nucleotide (see the conformation of dCTP in

DOI: 10.1021/bi5014936
Biochemistry 2015, 54, 639−651

Table 5. Crystal Data Collection and Refinement Statistics for Ternary Complexes Dpo4-1 (Dpo4:*S*-cdG:dCTP, PDB entry 4TQS) and Dpo4-2 (Dpo4:*S*-cdG:dTTP, PDB entry 4TQR)

	Dpo4-1 (4TQS)	Dpo4-2 (4TQR)
Data Collection		
template:dNTP	*S*-cdG:dCTP	*S*-cdG:dTTP
beamline	21-ID-F	21-ID-F
space group	$P2_1$	$P2_12_12_1$
unit cell (a, b, c) (Å)	52.12, 184.24, 52.12	58.54, 89.41, 112.39
unit cell (α, β, γ) (deg)	90.00, 110.00, 90.00	90.00, 90.00, 90.00
resolution range (Å)[a]	28.41−2.06 (2.10−2.06)	28.32−1.58 (1.60−1.58)
no. of unique reflections	55908	81191
completeness (%)	98.5 (98.5)	99.7 (99.9)
redundancy	3.8 (3.4)	5.5 (5.0)
R_{linear}[b]	0.088 (0.41)	0.057 (0.50)
signal to noise ($I/\sigma I$)	13.9 (3.0)	23.0 (2.9)
coordinate composition (asymmetric unit)		
no. of protein molecules	2	1
no. of amino acid residues	685	342
no. of water molecules	491	561
no. of Mg^{2+} ions	4	3
no. of Ca^{2+} ions	0	2
no. of template nucleotides	27	18
no. of primer nucleotides	26	13
no. of dCTPs	2	0
no. of dTTPs	0	1
Refinement		
resolution range (Å)	28.41−2.06	28.32−1.58
no. of reflections	53191	77167
R_{work} (%)[c]	22.8	18.2
R_{free} (%)[d]	28.9	20.2
rmsd for bond lengths (Å)	0.009	0.007
rmsd for bond angles (deg)	1.1	1.2
average B (Å)	26.4	34.0
Wilson B (Å)	20.2	19.8
Ramachandran summary		
amino acids in preferred regions	651 (95.6%)	331 (97.4%)
amino acids in allowed regions	21 (3.1%)	8 (2.4%)
outliers	9 (1.3%)	1 (0.29%)

[a]Values for the highest-resolution bin are given in parentheses. [b]$R_{linear} = \sum|I - \langle I\rangle|/\sum I$, where I is the integrated intensity of a given reflection. [c]$R_f = \sum|F_{observed} - F_{calculated}|/\sum|F_{observed}|$. [d]$R_{free}$ was calculated using a 5% test size with random selection.

Figure 6A for comparison). This unusual conformation of dTTP is facilitated by several interactions: (i) the pyrimidine ring interacted with template A at position +2 via $\pi-\pi$ interactions, (ii) the methyl−π interactions occurred between the pyrimidine ring and the methyl group of dTTP (Figure 6F), and (iii) two magnesium ions chelated the phosphate groups (Figure 6G). As shown in Figure 6G, a second magnesium also chelated the exocyclic oxygen atom of template C at position +3 in addition to interacting with Glu106, Asp7, the oxygen of dTTP β-phosphate, and two water molecules. Notably, Dpo4-2 was also catalytically incompetent, consistent with the low specificity constant of dTTP observed in the steady-state assays. Together, structures of Dpo4-1 and Dpo4-2 provided structural evidence of the existence of the inactive complex. Importantly, the looped template potentially induced by *S*-cdG in Dpo4-2 is consistent with the previously proposed CPU-induced secondary structures evidenced by the nuclease footprinting assay.[53] The catalytically null complexes are in agreement with the low bypass efficiencies in the primer extension and steady-state assays. Transient productive conformations are likely to exist in equilibrium with nonproductive complexes,[56] because small amounts of bypass products were indeed observed for Dpo1 and Dpo4.

We attempted to capture the *S*-cdG at the active site base pairing with an incoming nucleotide and were unsuccessful. Other conditions have all been recalcitrant to crystallization, including (i) a ternary complex with a 13-mer primer terminated with a regular 2′-deoxycytidine and an inhibitor 2′-deoxycytidine-5′-[(α,β)-imido]triphosphate (dCMPNPP), (ii) a binary complex with a 13-mer primer terminated with a regular 2′-deoxycytidine and an inhibitor 2′-dideoxycytidine triphosphate, and (iii) a binary complex with a 14/18-mer containing *S*-cdG. It is likely that the Dpo4:DNA(*S*-cdG):dNTP complex adopts multiple conformations that exist in equilibrium.[52] This is evidenced by (i) a substoichiometric burst (1%) in Dpo4-catalyzed dCTP insertion opposite *S*-cdG (Table 2 and Figure 4) and (ii) a potentially reversible nucleotidyl transfer [step 4 in Scheme 1; *vide supra* product amplitude was dependent on dCTP concentration (Table 3 and Figure S2F of the Supporting Information)].

DOI: 10.1021/bi5014936
Biochemistry 2015, 54, 639−651

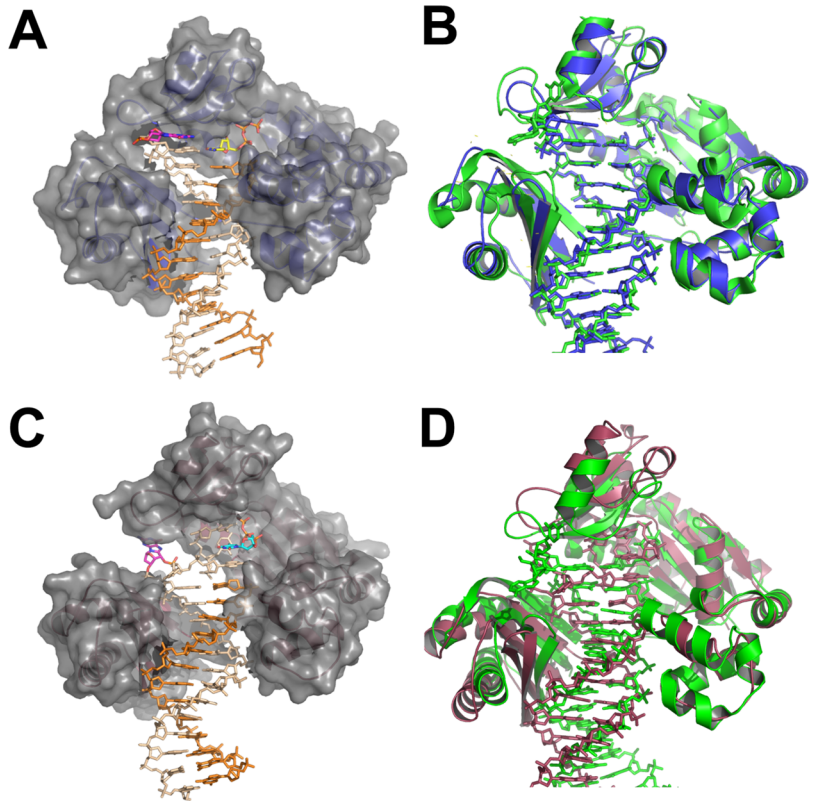

Figure 5. Overall architecture of cocrystal structures of Dpo4:*S*-cdG:dCTP (PDB entry 4TQS) and Dpo4:*S*-cdG:dTTP (PDB entry 4TQR). Surface view of Dpo4 with the DNA duplex containing *S*-cdG and an incoming nucleotide dCTP (A) or dTTP (C). Superimposed structures of Dpo4:*S*-cdG:dCTP (B) or Dpo4:*S*-cdG:dTTP (D) (both colored red) with a previously determined Dpo4 structure (green, PDB entry 2C2R).

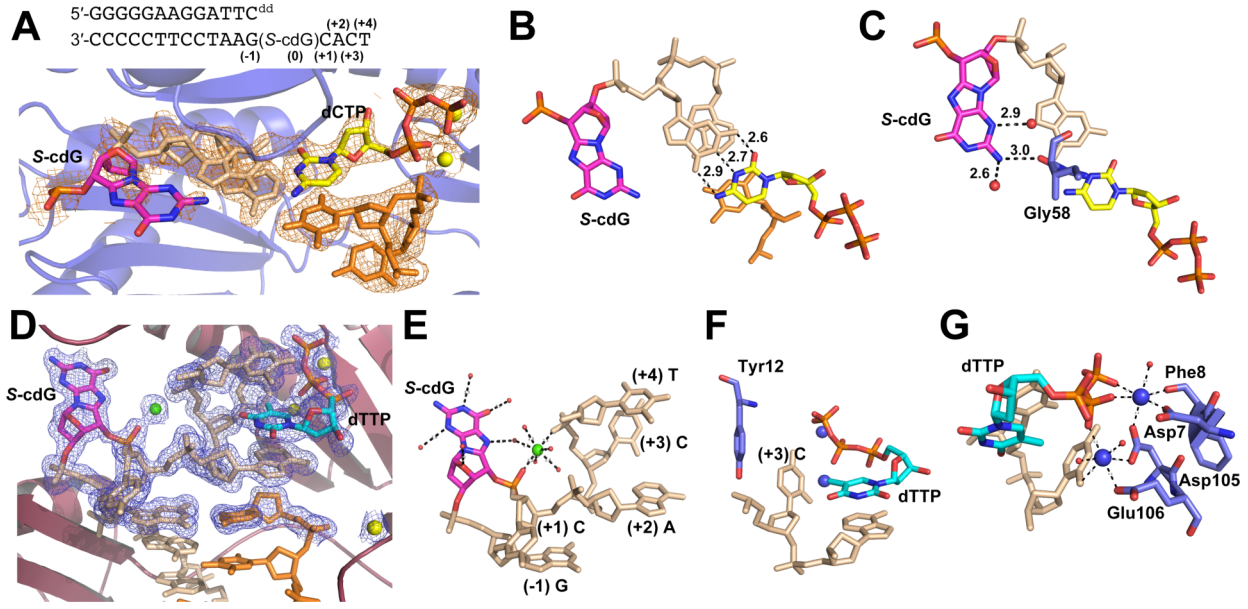

Figure 6. Close-up view of the active site of Dpo4:*S*-cdG:dNTP complexes. (A) The Dpo4:*S*-cdG:dCTP complex with an unbiased simulated annealing omit map shown at 1σ (orange mesh). (B) The incoming dCTP is paired with G at position −1 (hydrogen bond length in angstroms). (C) *S*-cdG interacted with Gly58 and two water molecules via hydrogen binding (distance in angstroms). Specifically, the exocyclic N2 atom of *S*-cdG formed hydrogen bonds with the carbonyl O atom of the Gly58 backbone, and the N3 atom of *S*-cdG formed a hydrogen bond with a water molecule. (D) Dpo4:*S*-cdG:dTTP complex with an unbiased simulated annealing omit map shown at the 1σ level (blue mesh). The *S*-cdG lesion induced a "loop" structure causing four three-template bases at positions +2, +3, and +4 clustered at the active site. The incoming dTTP was displaced from the typical position for an incoming nucleotide seen in a "type I" Dpo4 structure. (E) The *S*-cdG lesion was stabilized by hydrogen bonds with several water molecules and Ca^{2+} chelation. (F) The template C at position +3 interacted with Tyr12 using hydrophobic interactions and shifted dTTP outside the active site. The dTTP stacked with the template A at position +2. (G) The incoming dTTP adopted a "goat-tail"-like conformation with two chelated Mg^{2+} ions.

DOI: 10.1021/bi5014936
Biochemistry 2015, 54, 639−651

DISCUSSION

The CPU lesions are among the major DNA lesions induced by ionizing radiation or endogenous reactive oxygen species. It is known that 8-oxodG can be efficiently removed via BER, whereas CPU lesions are excised through NER with low efficiency.[25,27,29] However, it is controversial in terms of the steady-state levels of CPU lesions compared to those of common oxidative DNA damage, 8-oxodG, mainly because artificial 8-oxodG can be generated during sample workup.[13,57] The levels of cdG lesions are approximately 2−4 orders of magnitude lower than those of 8-oxodG in vitro induced by Fenton-type reagents.[58] Under oxidative stress, the levels of CPU lesions in mouse models were found to be approximately 1 per 10^6 nucleosides.[19,20] Because CPU lesions are resistant to repair compared to 8-oxodG, it is conceivable that the level of CPU in vivo may not be that low compared to that of 8-oxodG, and CPU lesions may contribute to disease etiology.

In vitro, *S*-cdA is a strong block to DNA replication by B-family pol δ and T7 DNA polymerase,[25] and *S*-cdG and *S*-cdA also block Y-family *E. coli* pol IV and Dpo4.[33] In *E. coli* cells, bypass efficiencies of *S*-cdG and *S*-cdA during replication are <5%.[29,59] Consistent with these findings, our primer extension assays have shown *S*-cdG blocked Dpo1- and Dpo4-catalyzed primer extensions (Figure 2 and Figure S1 of the Supporting Information) and postlesion DNA synthesis (Table 4 and Figure S3 of the Supporting Information). In *E. coli* cells, *S*-cdG induces G → A transition (20%) and G → T transversion (80%) mutations,[29,59] whereas in human 293T cells, *S*-cdG induces a 50% higher total mutation frequency and a G → T mutation frequency higher than the G → A mutation frequency.[32] Misincorporation patterns observed for Dpo1 and Dpo4 agree with reported mutations: Dpo1 misinserted A (misincorporation frequency of 0.11), and Dpo4 misinserted T [misincorporation frequency of 0.37 (Table 1)], although dCTP was the preferred nucleotide of both pols. Compared to that for replications opposite unmodified G, the specificity constant for the insertion of correct dCTP across *S*-cdG decreased 65-fold for Dpo4 and 140-fold for Dpo1. In a different template sequence and under the catalysis of Dpo4, *S*-cdG attenuated dCTP insertion by 440-fold, and the dTTP misinsertion frequency was 0.29, suggesting that catalytic efficiency and misincorporation frequency were sequence-dependent (Table S1 of the Supporting Information). Indeed, Pednekar et al. used a different *S*-cdG-bearing template sequence and found a 10-fold higher frequency of misinsertion of dTTP by Dpo4 compared to insertion of dCTP opposite *S*-cdG.[33] As suggested by a recent study[53] and also evidenced by our structural data, such sequence-dependent catalytic efficiency differences may be derived from the different secondary structures (e.g., loop or hairpin) formed in different CPU-harboring templates.

This study provides mechanistic insights into how *S*-cdG causes DNA replication stalling. We discuss the effects imposed by *S*-cdG using a minimal kinetic model (Scheme 1, steps 1−6).[38,60,61] An additional step (step 7 in Scheme 1) is included during *S*-cdG bypass as suggested by previous kinetic studies examining bypass of other lesions.[50,56,62] A DNA lesion can perturb the normal mechanism for fidelity and efficiency, producing nonproductive ternary complexes (Scheme 1, step 7), mutagenic mispairs, or polymerase stalling.[63] The specificity constant (k_{cat}/K_m in Table 1) is a function of all kinetic steps in a single catalytic cycle and is often limited by DNA product release for replicative DNA polymerases[63] or a conformational relaxation step after the nucleotidyl transfer for translesion DNA polymerases, such as Dpo4 and human pol κ.[38,50]

Kinetic investigations of the microscopic catalytic steps revealed that *S*-cdG compromised the bypass of Dpo1 and Dpo4 through different mechanisms. *S*-cdG disturbed catalytic steps 2−4 (Table 3) for Dpo1, but not step 1 (pol−DNA binding, Figure 3). The presence of *S*-cdG in the template did not considerably alter the partitioning between the productive and unproductive Dpo1:DNA(*S*-cdG):dCTP complex (Table 2).[63] For Dpo4-catalyzed insertion of dCTP opposite *S*-cdG, the lesion compromised pol−DNA binding (Figure 3) and decreased the concentration of the productive Dpo4:DNA(*S*-cdG):dCTP complex by approximately 100-fold (Table 2), resulting in a 65-fold decrease in catalytic efficiency compared to that of a duplex without the lesion (in Table 1). The dCTP catalytic efficiency ($k_{pol}/K_{d,dCTP,app}$) for Dpo4 across *S*-cdG is 15-fold higher than that across dG. A higher efficiency was also reported for Dpo4-catalyzed insertion of dCTP opposite template 8-oxodG compared to the dG:dCTP pair, but not for adducted templates containing O^6-benzylguanine or N^2-benzylguanine adduct,[63,64] suggesting versatile catalytic mechanisms exist for TLS pols in various lesion bypass scenarios. Our results support a model in which Dpo1-catalyzed replication is blocked by the lesion, and Dpo4 is recruited to incorporate a single base across the lesion (Dpo4 showed a 73-fold higher $k_{pol}/K_{d,dCTP,app}$ compared to that of Dpo1), followed by Dpo1 taking over during postlesion DNA synthesis (higher postlesion extension efficiency seen for Dpo1 in Table 4). Dpo1 may also proofread the *S*-cdG:dNTP pair with 3′ → 5′ exonuclease activity to further improve fidelity.[6]

Our crystallographic data provided the first structural insight into translesion DNA synthesis across *S*-cdG. Both dCTP- and dTTP-complexed Dpo4 crystal structures were catalytically incompetent, consistent with the inefficient bypass observed. Changes in template backbone torsion angles induced by *S*-cdG may contribute to the shift of *S*-cdG outside the active site.[34−36] In the Dpo4:*S*-cdG:dCTP structure, interactions with Gly58 and several water molecules may hinder strand translocation and inhibit bypass activity. Recently, Liu and her colleagues found that cdA can induce the formation of loop structures of varying sizes on the template strand.[53] Indeed, we discovered the *S*-cdG-harboring template formed a looplike structure in the Dpo4:*S*-cdG:dTTP complex, which provided some structural evidence of the Dpo4 replication stalling caused by *S*-cdG, and perhaps can also contribute to the DNA polymerase stalling seen for other B-family and Y-family polymerases.

In summary, we have deciphered novel kinetic and structural mechanisms pertaining to CPU lesion-induced DNA polymerase stalling. Our results provided several lines of evidence of the structure−function relationship of CPU lesion bypass. We demonstrated that the *S*-cdG lesion caused unusual interactions with a Dpo4 active site residue or a template clustering during bypass. It is likely that a similar structural disruption imposed by CPU lesions could also contribute to the DNA replication stalling by other eukaryotic DNA polymerases.

ASSOCIATED CONTENT

Supporting Information

Steady-state kinetic parameters with a 16/23-mer duplex (Table S1), primer extension assay images (Figures S1 and S3), and data and fit for pre-steady-state kinetics under single-turnover

DOI: 10.1021/bi5014936
Biochemistry 2015, 54, 639−651

conditions (Figure S2). This material is available free of charge via the Internet at http://pubs.acs.org.

Accession Codes

The coordinates and structural factors of ternary complexes Dpo4-1 (Dpo4:*S*-cdG:dCTP, PDB entry 4TQS) and Dpo4-2 (Dpo4:*S*-cdG:dTTP, PDB entry 4TQR) have been deposited in the RCSB Protein Data Bank.

AUTHOR INFORMATION

Corresponding Author

*E-mail: linlin.zhao@cmich.edu. Telephone: (989) 774-3252. Fax: (989) 774-3883.

Funding

This work was supported by Central Michigan University start-up funds (to L.Z.) and ResearchRewards from TriLink Biotechnologies (to L.Z.). Use of the Advanced Photon Source, an Office of Science User Facility operated for the U.S. Department of Energy (DOE) Office of Science by Argonne National Laboratory, was supported by the U.S. DOE under Contract DE-AC02-06CH11357. Use of LS-CAT Sector 21 was supported by the Michigan Economic Development Corp. and the Michigan Technology Tri-Corridor (Grant 085P1000817).

Notes

The authors declare no competing financial interest.

ACKNOWLEDGMENTS

We are grateful to Prof. F. Peter Guengerich for providing Dpo1 (exo$^-$) and Dpo4 expression plasmids. We thank Prof. Martin Egli and Dr. Matthew G. Pence for critically reading the manuscript and Dr. Wei Yang for helpful discussions about crystallization conditions.

ABBREVIATIONS

BER, base excision repair; BSA, bovine serum albumin; C^{dd}, 2′,3′-dideoxycytidine; cdA, 8,5′-cyclo-2′-deoxyadenosine; cdG, 8,5′-cyclo-2′-deoxyguanosine; CPU, cyclopurine; Dpo1, *S. solfataricus* P2 DNA polymerase B1; Dpo4, *S. solfataricus* P2 DNA polymerase IV; DTT, dithiothreitol; exo$^-$, exonuclease-deficient; FAM, fluorescein amidite; NER, nucleotide excision repair; pol, DNA polymerase; 8-oxodG, 8-oxo-7,8-dihydro-2′-deoxyguanosine; *S*-cdG, (5′*S*)-8,5′-cyclo-2′-deoxyguanosine; *Sso*., *S. solfataricus* P2; TLS, translesion DNA synthesis.

REFERENCES

(1) Hübscher, U., and Maga, G. (2011) DNA replication and repair bypass machines. *Curr. Opin. Chem. Biol. 15*, 627−635.

(2) Sale, J. E. (2013) Translesion DNA synthesis and mutagenesis in eukaryotes. *Cold Spring Harbor Perspect. Biol. 5*, a012708.

(3) Hoeijmakers, J. H. J. (2001) Genome maintenance mechanisms for preventing cancer. *Nature 411*, 366−374.

(4) Trakselis, M. A., and Bauer, R. J. (2014) Archaeal DNA polymerases: Enzymatic abilities, coordination, and unique properties. In *Nucleic Acid Polymerases*, pp 139−162, Springer, Berlin.

(5) Choi, J.-Y., Eoff, R. L., Pence, M. G., Wang, J., Martin, M. V., Kim, E.-J., Folkmann, L. M., and Guengerich, F. P. (2011) Roles of the four DNA polymerases of the crenarchaeon *Sulfolobus solfataricus* and accessory proteins in DNA replication. *J. Biol. Chem. 286*, 31180−31193.

(6) Zhang, L., Brown, J. A., Newmister, S. A., and Suo, Z. (2009) Polymerization fidelity of a replicative DNA polymerase from the hyperthermophilic archaeon *Sulfolobus solfataricus* P2. *Biochemistry 48*, 7492−7501.

(7) Grúz, P., Shimizu, M., Pisani, F. M., Felice, M. D., Kanke, Y., and Nohmi, T. (2003) Processing of DNA lesions by archaeal DNA polymerases from *Sulfolobus solfataricus*. *Nucleic Acids Res. 31*, 4024−4030.

(8) Ling, H., Boudsocq, F., Woodgate, R., and Yang, W. (2001) Crystal structure of a Y-family DNA polymerase in action: A mechanism for error-prone and lesion-bypass replication. *Cell 107*, 91−102.

(9) Ling, H., Boudsocq, F., Plosky, B. S., Woodgate, R., and Yang, W. (2003) Replication of a *cis-syn* thymine dimer at atomic resolution. *Nature 424*, 1083−1087.

(10) Ling, H., Sayer, J. M., Plosky, B. S., Yagi, H., Boudsocq, F., Woodgate, R., Jerina, D. M., and Yang, W. (2004) Crystal structure of a benzo[*a*]pyrene diol epoxide adduct in a ternary complex with a DNA polymerase. *Proc. Natl. Acad. Sci. U.S.A. 101*, 2265−2269.

(11) Eoff, R. L., Irimia, A., Angel, K., Egli, M., and Guengerich, F. P. (2007) Hydogen bonding of 7,8-dihydro-8-oxodeoxyguanosine with a charged residue in the little finger domain determines miscoding events in *Sulfolobus solfataricus* DNA polymerase Dpo4. *J. Biol. Chem. 282*, 19831−19843.

(12) Jaruga, P., and Dizdaroglu, M. (2008) 8,5′-Cyclopurine-2′-deoxynucleosides in DNA: Mechanisms of formation, measurement, repair and biological effects. *DNA Repair 7*, 1413−1425.

(13) Chatgilialoglu, C., Ferreri, C., and Terzidis, M. A. (2011) Purine 5′,8-cyclonucleoside lesions: Chemistry and biology. *Chem. Soc. Rev. 40*, 1368−1382.

(14) Keck, K. (1968) Formation of cyclonucleotides during irradiation of aqueous solutions of purine nucleotides. *Z. Naturforsch. B23*, 1034−1043.

(15) Dizdaroglu, M. (1986) Free-radical-induced formation of an 8,5′-cyclo-2′-deoxyguanosine moiety in deoxyribonucleic acid. *Biochem. J. 238*, 247−254.

(16) Randerath, K., Zhou, G.-D., Somers, R. L., Robbins, J. H., and Brooks, P. J. (2001) A ^{32}P-postlabeling assay for the oxidative DNA lesion 8,5′-cyclo-2′-deoxyadenosine in mammalian tissues evidence that four Type II I-compounds are dinucleotides containing the lesion in the 3′ nucleotide. *J. Biol. Chem. 276*, 36051−36057.

(17) Wang, J., Yuan, B., Guerrero, C., Bahde, R., Gupta, S., and Wang, Y. (2011) Quantification of oxidative DNA lesions in tissues of long-evans cinnamon rats by capillary high-performance liquid chromatography-tandem mass spectrometry coupled with stable isotope-dilution method. *Anal. Chem. 83*, 2201−2209.

(18) Wang, J., Clauson, C. L., Robbins, P. D., Niedernhofer, L. J., and Wang, Y. (2012) The oxidative DNA lesions 8,5′-cyclopurines accumulate with aging in a tissue-specific manner. *Aging Cell 11*, 714−716.

(19) Shaked, H., Hofseth, L. J., Chumanevich, A., Chumanevich, A. A., Wang, J., Wang, Y., Taniguchi, K., Guma, M., Shenouda, S., Clevers, H., Harris, C. C., and Karin, M. (2012) Chronic epithelial NF-κB activation accelerates APC loss and intestinal tumor initiation through iNOS up-regulation. *Proc. Natl. Acad. Sci. U.S.A. 109*, 14007−14012.

(20) Tilstra, J. S., Robinson, A. R., Wang, J., Gregg, S., Clauson, C. L., Reay, D. P., Nasto, L. A., St Croix, C. M., Usas, A., Vo, N., Huard, J., Clemens, P. R., Stolz, D. B., Guttridge, D. C., Watkins, S. C., Garinis, G. A., Wang, Y., Niedernhofer, L. J., and Robbins, P. D. (2012) NF-κB inhibition delays DNA damage-induced senescence and aging in mice. *J. Clin. Invest. 122*, 2601−2612.

(21) Mitra, D., Luo, X., Morgan, A., Wang, J., Hoang, M. P., Lo, J., Guerrero, C. R., Lennerz, J. K., Mihm, M. C., Wargo, J. A., Robinson, K. C., Devi, S. P., Vanover, J. C., D'Orazio, J. A., McMahon, M., Bosenberg, M. W., Haigis, K. M., Haber, D. A., Wang, Y., and Fisher, D. E. (2012) An ultraviolet-radiation-independent pathway to melanoma carcinogenesis in the red hair/fair skin background. *Nature 491*, 449−453.

(22) Kirkali, G., Tunca, M., Genc, S., Jaruga, P., and Dizdaroglu, M. (2008) Oxidative DNA damage in polymorphonuclear leukocytes of patients with familial Mediterranean fever. *Free Radical Biol. Med. 44*, 386−393.

DOI: 10.1021/bi5014936
Biochemistry 2015, 54, 639−651

(23) Kirkali, G., de Souza-Pinto, N. C., Jaruga, P., Bohr, V. A., and Dizdaroglu, M. (2009) Accumulation of (5′*S*)-8,5′-cyclo-2′-deoxyadenosine in organs of Cockayne syndrome complementation group B gene knockout mice. *DNA Repair 8*, 274−278.
(24) Brooks, P. J. (2008) The 8,5′-cyclopurine-2′-deoxynucleosides: Candidate neurodegenerative DNA lesions in xeroderma pigmentosum, and unique probes of transcription and nucleotide excision repair. *DNA Repair 7*, 1168−1179.
(25) Kuraoka, I., Bender, C., Romieu, A., Cadet, J., Wood, R. D., and Lindahl, T. (2000) Removal of oxygen free-radical-induced 5′,8-purine cyclodeoxynucleosides from DNA by the nucleotide excision-repair pathway in human cells. *Proc. Natl. Acad. Sci. U.S.A. 97*, 3832−3837.
(26) Pande, P., Das, R. S., Sheppard, C., Kow, Y. W., and Basu, A. K. (2012) Repair efficiency of (5′*S*)-8,5′-cyclo-2′-deoxyguanosine and (5′*S*)-8,5′-cyclo-2′-deoxyadenosine depends on the complementary base. *DNA Repair 11*, 926−931.
(27) Brooks, P. J., Wise, D. S., Berry, D. A., Kosmoski, J. V., Smerdon, M. J., Somers, R. L., Mackie, H., Spoonde, A. Y., Ackerman, E. J., and Coleman, K. (2000) The oxidative DNA lesion 8,5′-(*S*)-cyclo-2′-deoxyadenosine is repaired by the nucleotide excision repair pathway and blocks gene expression in mammalian cells. *J. Biol. Chem. 275*, 22355−22362.
(28) Jaruga, P., Xiao, Y., Vartanian, V., Lloyd, R. S., and Dizdaroglu, M. (2010) Evidence for the involvement of DNA repair enzyme NEIL1 in nucleotide excision repair of (5′*R*)- and (5′*S*)-8,5′-cyclo-2′-deoxyadenosines. *Biochemistry 49*, 1053−1055.
(29) Jasti, V. P., Das, R. S., Hilton, B. A., Weerasooriya, S., Zou, Y., and Basu, A. K. (2011) (5′*S*)-8,5′-Cyclo-2′-deoxyguanosine is a strong block to replication, a potent pol V-dependent mutagenic lesion, and is inefficiently repaired in *Escherichia coli*. *Biochemistry 50*, 3862−3865.
(30) Kropachev, K., Ding, S., Terzidis, M. A., Masi, A., Liu, Z., Cai, Y., Kolbanovskiy, M., Chatgilialoglu, C., Broyde, S., and Geacintov, N. E. (2014) Structural basis for the recognition of diastereomeric 5′,8-cyclo-2′-deoxypurine lesions by the human nucleotide excision repair system. *Nucleic Acids Res. 42*, 5020−5032.
(31) Marietta, C., Gulam, H., and Brooks, P. J. (2002) A single 8,5′-cyclo-2′-deoxyadenosine lesion in a TATA box prevents binding of the TATA binding protein and strongly reduces transcription in vivo. *DNA Repair 1*, 967−975.
(32) You, C., Swanson, A. L., Dai, X., Yuan, B., Wang, J., and Wang, Y. (2013) Translesion synthesis of 8,5′-cyclopurine-2′-deoxynucleosides by DNA polymerases *η*, *ι*, and *ζ*. *J. Biol. Chem. 288*, 28548−28556.
(33) Pednekar, V., Weerasooriya, S., Jasti, V. P., and Basu, A. K. (2014) Mutagenicity and Genotoxicity of (5′*S*)-8,5′-Cyclo-2′-deoxyadenosine in *Escherichia coli* and Replication of (5′*S*)-8,5′-Cyclopurine-2′-deoxynucleosides in Vitro by DNA Polymerase IV, Exo-Free Klenow Fragment, and Dpo4. *Chem. Res. Toxicol. 27*, 200−210.
(34) Huang, H., Das, R. S., Basu, A. K., and Stone, M. P. (2011) Structure of (5′*S*)-8,5′-cyclo-2′-deoxyguanosine in DNA. *J. Am. Chem. Soc. 133*, 20357−20368.
(35) Huang, H., Das, R. S., Basu, A. K., and Stone, M. P. (2012) Structures of (5′*S*)-8,5′-Cyclo-2′-deoxyguanosine Mismatched with dA or dT. *Chem. Res. Toxicol. 25*, 478−490.
(36) Zaliznyak, T., Lukin, M., and de los Santos, C. (2012) Structure and stability of duplex DNA containing (5′*S*)-5′,8-cyclo-2′-deoxyadenosine: An oxidatively generated lesion repaired by NER. *Chem. Res. Toxicol. 25*, 2103−2111.
(37) Zang, H., Goodenough, A. K., Choi, J. Y., Irimia, A., Loukachevitch, L. V., Kozekov, I. D., Angel, K. C., Rizzo, C. J., Egli, M., and Guengerich, F. P. (2005) DNA adduct bypass polymerization by *Sulfolobus solfataricus* DNA polymerase Dpo4: Analysis and crystal structures of multiple base pair substitution and frameshift products with the adduct 1,N^2-ethenoguanine. *J. Biol. Chem. 280*, 29750−29764.
(38) Zhao, L., Pence, M. G., Eoff, R. L., Yuan, S., Fercu, C. A., and Guengerich, F. P. (2014) Elucidation of kinetic mechanisms of human translesion DNA polymerase *κ* using tryptophan mutants. *FEBS J. 281*, 4394−4410.
(39) Johnson, A. A., Ray, A. S., Hanes, J., Suo, Z., Colacino, J. M., Anderson, K. S., and Johnson, K. A. (2001) Toxicity of antiviral nucleoside analogs and the human mitochondrial DNA polymerase. *J. Biol. Chem. 276*, 40847−40857.
(40) Zhao, L., Christov, P. P., Kozekov, I. D., Pence, M. G., Pallan, P. S., Rizzo, C. J., Egli, M., and Guengerich, F. P. (2012) Replication of N^2,3-ethenoguanine by DNA polymerases. *Angew. Chem., Int. Ed. 51*, 5466−5469.
(41) Otwinowski, Z., and Minor, W. (1997) Processing of X-ray diffraction data collected in oscillation mode. *Methods Enzymol. 276*, 307−326.
(42) Vagin, A., and Teplyakov, A. (1997) MOLREP: An automated program for molecular replacement. *J. Appl. Crystallogr. 30*, 1022−1025.
(43) Fiala, K. A., Brown, J. A., Ling, H., Kshetry, A. K., Zhang, J., Taylor, J. S., Yang, W., and Suo, Z. (2007) Mechanism of template-independent nucleotide incorporation catalyzed by a template-dependent DNA polymerase. *J. Mol. Biol. 365*, 590−602.
(44) Winn, M. D., Ballard, C. C., Cowtan, K. D., Dodson, E. J., Emsley, P., Evans, P. R., Keegan, R. M., Krissinel, E. B., Leslie, A. G. W., and McCoy, A. (2011) Overview of the CCP4 suite and current developments. *Acta Crystallogr. D67*, 235−242.
(45) Lamzin, V. S., and Wilson, K. S. (1993) Automated refinement of protein models. *Acta Crystallogr. D49*, 129−147.
(46) Adams, P. D., Afonine, P. V., Bunkoczi, G., Chen, V. B., Davis, I. W., Echols, N., Headd, J. J., Hung, L.-W., Kapral, G. J., Grosse-Kunstleve, R. W., McCoy, A. J., Moriarty, N. W., Oeffner, R., Read, R. J., Richardson, D. C., Richardson, J. S., Terwilliger, T. C., and Zwart, P. H. (2010) PHENIX: A comprehensive Python-based system for macromolecular structure solution. *Acta Crystallogr. D66*, 213−221.
(47) Emsley, P., and Cowtan, K. (2004) Coot: Model-building tools for molecular graphics. *Acta Crystallogr. D60*, 2126−2132.
(48) DeLano, W. L. (2002) *The PyMOL Molecular Graphics System*, DeLano Scientific, San Carlos, CA.
(49) Maxwell, B. A., and Suo, Z. (2012) Kinetic basis for the differing response to an oxidative lesion by a replicative and a lesion bypass DNA polymerase from *Sulfolobus solfataricus*. *Biochemistry 51*, 3485−3496.
(50) Beckman, J. W., Wang, Q., and Guengerich, F. P. (2008) Kinetic analysis of nucleotide insertion by a Y-family DNA polymerase reveals conformational change both prior to and following phosphodiester bond formation as detected by tryptophan fluorescence. *J. Biol. Chem. 283*, 36711−36723.
(51) Zang, H., Irimia, A., Choi, J.-Y., Angel, K. C., Loukachevitch, L. V., Egli, M., and Guengerich, F. P. (2006) Efficient and High Fidelity Incorporation of dCTP Opposite 7,8-Dihydro-8-oxodeoxyguanosine by *Sulfolobus solfataricus* DNA Polymerase Dpo4. *J. Biol. Chem. 281*, 2358−2372.
(52) Ling, H., Boudsocq, F., Woodgate, R., and Yang, W. (2004) Snapshots of replication through an abasic lesion: Structural basis for base substitutions and frameshifts. *Mol. Cell 13*, 751−762.
(53) Xu, M., Lai, Y., Jiang, Z., Terzidis, M. A., Masi, A., Chatgilialoglu, C., and Liu, Y. (2014) A 5′,8-cyclo-2′-deoxypurine lesion induces trinucleotide repeat deletion via a unique lesion bypass by DNA polymerase *β*. *Nucleic Acids Res. 42*, 13749−13763.
(54) Vaisman, A., Ling, H., Woodgate, R., and Yang, W. (2005) Fidelity of Dpo4: Effect of metal ions, nucleotide selection and pyrophosphorolysis. *EMBO J. 24*, 2957−2967.
(55) Harding, M. (1999) The geometry of metal-ligand interactions relevant to proteins. *Acta Crystallogr. D55*, 1432−1443.
(56) Fiala, K. A., Hypes, C. D., and Suo, Z. (2007) Mechanism of abasic lesion bypass catalyzed by a Y-family DNA polymerase. *J. Biol. Chem. 282*, 8188−8198.
(57) Cadet, J., Bellon, S., Berger, M., Bourdat, A.-G., Douki, T., Duarte, V., Frelon, S., Gasparutto, D., Muller, E., and Ravanat, J.-L. (2002) Recent aspects of oxidative DNA damage: Guanine lesions, measurement and substrate specificity of DNA repair glycosylases. *Biol. Chem. 383*, 933−943.

DOI: 10.1021/bi5014936
Biochemistry 2015, 54, 639−651

(58) Guerrero, C. R., Wang, J., and Wang, Y. (2013) Induction of 8,5′-cyclo-2′-deoxyadenosine and 8,5′-cyclo-2′-deoxyguanosine in isolated DNA by Fenton-type reagents. *Chem. Res. Toxicol. 26*, 1361−1366.
(59) Yuan, B., Wang, J., Cao, H., Sun, R., and Wang, Y. (2011) High-throughput analysis of the mutagenic and cytotoxic properties of DNA lesions by next-generation sequencing. *Nucleic Acids Res. 39*, 5945−5954.
(60) Roettger, M. P., Bakhtina, M., Kumar, S., and Tsai, M.-D. (2010) 8.10: Catalytic Mechanism of DNA Polymerases. In *Comprehensive Natural Products II* (Liu, H.-W., and Mander, L., Eds.) pp 349−383, Elsevier, Oxford, U.K.
(61) Showalter, A. K., and Tsai, M.-D. (2002) A reexamination of the nucleotide incorporation fidelity of DNA polymerases. *Biochemistry 41*, 10571−10576.
(62) Maxwell, B. A., and Suo, Z. (2014) Recent Insight into the Kinetic Mechanisms and Conformational Dynamics of Y-Family DNA Polymerases. *Biochemistry 53*, 2804−2814.
(63) Woodside, A. M., and Guengerich, F. P. (2002) Misincorporation and stalling at O^6-methylguanine and O^6-benzylguanine: Evidence for inactive polymerase complexes. *Biochemistry 41*, 1039−1050.
(64) Zhang, H., Eoff, R. L., Kozekov, I. D., Rizzo, C. J., Egli, M., and Guengerich, F. P. (2009) Versatility of Y-family *Sulfolobus solfataricus* DNA polymerase Dpo4 in translesion synthesis past bulky N^2-alkylguanine adducts. *J. Biol. Chem. 284*, 3563−3576.

DOI: 10.1021/bi5014936
Biochemistry 2015, 54, 639−651